ELSEVIER

Marine Structures **9** (1996) 151–179

0951-8339/96/$9.50

0951-8339(94)00010-7

Two-phase Finite Element Comparative Study of a Side Structure of a Middle Size Tanker

Y. Sumi†

Department of Naval Architecture and Ocean Engineering, Yokohama National University, 156 Tokiwadai, Hodogaya-ku, Yokohama 240, Japan

D. Cervetto†

Registro Italiano Navale, Genoa, Italy

P. K. Das†

University of Glasgow, UK

M. Hakala†

Technical Research Center of Finland, Espoo, Finland

R. Løseth†

Veritas Research, Høvik, Norway

N. Pegg†

Defence Research Establishment Atlantic, Dartmouth, Canada

I. Senjanovic†

University of Zagreb, Croatia

R. Sielski†

Marine Board, National Research Council, Washington DC, USA

W. Wang†

National Taiwan Ocean University, Keelung, Taiwan, Republic of China

†members of ISSC '94 Committee II.1, editor Y. Sumi.

P. Rigo

University of Liege, Belgium

T. Kushima

Sumitomo Heavy Industries, Yokosuka, Japan

&

B. Snyder

Naval Surface Warfare Center, Carderock, MD, USA

(Received 7 July 1994)

ABSTRACT

A comparative study of a two-phase finite element structural analysis has been undertaken by members of Technical Committee II.1 of ISSC '94. A side structure of a middle size crude oil carrier was taken as a typical example of an orthogonally stiffened panel structure. The first phase of the analysis was the global deformation and stress analysis of the side structure, while the second phase was the local stress analysis at the intersection of a transverse frame and a longitudinal stiffener. The numerical results are summarized, and investigations are made for the possible sources of the differences observed in the study.

Key words: comparative study, finite element structural analysis, a side structure of a tanker.

1 INTRODUCTION

The finite element (FE) method has commonly been used as a standard procedure to analyze the response of a large variety of engineering structures. By using this method, ship structural designers can calculate stresses and displacements of ship hulls and structural details, the degree of accuracy of which may vary with the solution procedure.

The results given by finite element analyses vary mainly due to structural idealizations, finite element mesh discretizations, and load and boundary conditions applied to the structural model. A structural designer should correctly understand the numerical results from finite element

analysis so that rational engineering judgements can be made in various aspects of structural design.

The importance of the FE comparative study has been recognized by Technical Committee II.1 of ISSC '94, and a two-phase structural analysis has been studied by using a side structure of a middle size crude oil carrier as a typical example of orthogonally stiffened panel structures. The first phase is the global analysis of the side structure, and the second phase is the evaluation of the local stresses at the connection of a longitudinal stiffener and a transverse frame. This analysis would be of the type used for determining stress details for fatigue. Nine committee members and some outside collaborators have contributed to this study. The problem was analyzed independently by each contributor using his own solution procedure. Based on the contributed results reported from individual contributors[1–11], the comparative study is presented herein.

The comparative study of this kind was initiated by a previous committee (Committee II.1 of ISSC '91) to make a further contribution to understanding the uncertainties associated with finite element analysis of ship structures.[12,13] They focused their attention on the comparisons of global deformations and nominal stresses. The present study further extends the approach to the two-phase evaluation of global and local deformations and stresses.

2 TWO-PHASE FINITE ELEMENT ANALYSIS

Structural data used for the analysis are obtained from the ship, whose principal particulars are given as

— DWT 88 000 tons,
— $L = 231\,\text{m}$, $B = 39{\cdot}4\,\text{m}$, $D = 18{\cdot}7\,\text{m}$, $d = 13{\cdot}9\,\text{m}$, $C_b = 0{\cdot}81$,

and whose tank arrangement is illustrated in Fig. 1. The ship was selected from the ship drawing collection of Department of Naval Architecture and Ocean Engineering, Yokohama National University.

The side structure of No. 2 side tank (water ballast tank) selected for the comparative study is illustrated in Fig. 2. Although an actual ship structure is used for the comparative study, it should be noted that the purpose of the present study is to investigate the variations of stresses and deformations due to the variety of structural idealization, applications of boundary conditions, and other hypotheses adopted by each contributor.

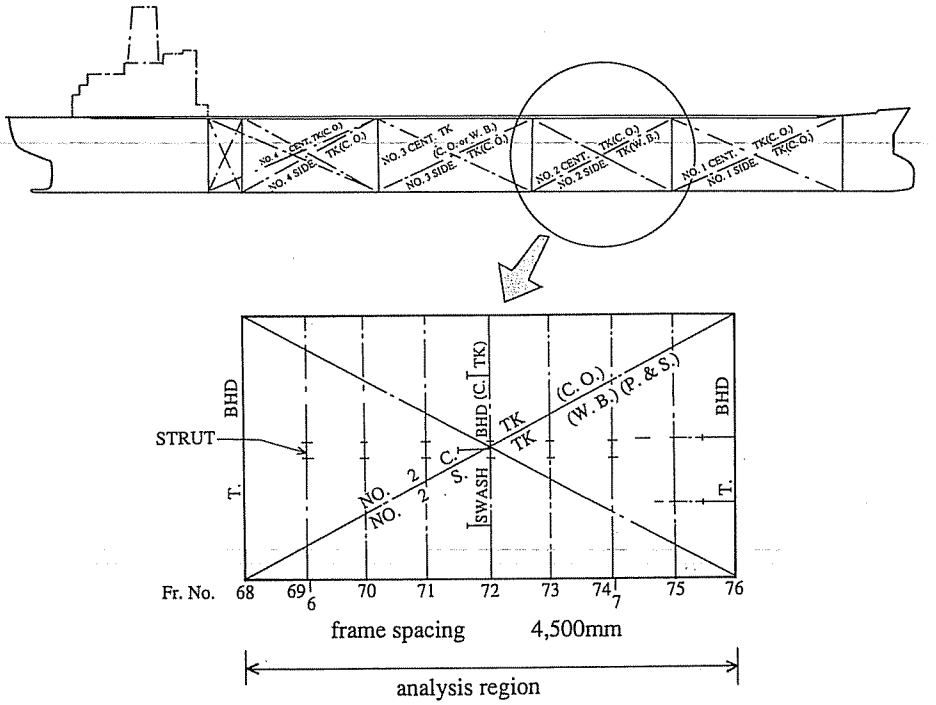

Fig. 1. Tank arrangement of a middle size tanker.

The structural analyses consisted of the two phases explained in the following subsections.

2.1 Phase-1 analysis

The first phase of the study was the analysis of the side structure extending from bulkhead to bulkhead and from deck to bottom, subjected to hydrostatic pressure. Deflections and the stresses calculated at certain points are compared. The results are investigated focusing on solution sensitivities due to the modeling of transverse frames (Frs) and longitudinal stiffeners (SLs), mesh refinement, and load applications.

Since No. 2 side tank is a water ballast tank, the extent of the region to be analyzed along with some common boundary conditions were assumed in the following manner;

(a) Extent of the analysis region:
from SL 1 to SL 20,
from T. Bulkhead to T. Bulkhead.

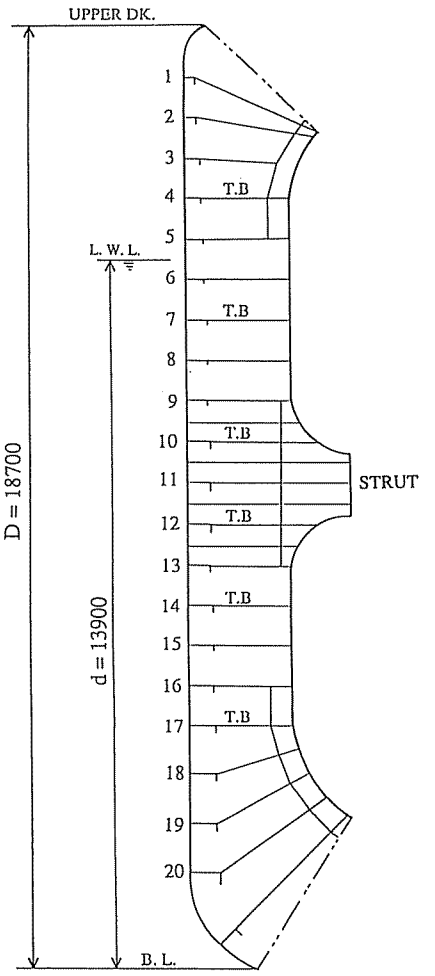

Fig. 2. Side structure.

(b) Boundary conditions:
simply supported at the intersections of the transverse frames with the struts,
simply supported along the transverse bulkheads,
simply supported along SL 1, fixed along SL 20.

(c) Loading condition:
subjected to external hydrostatic pressure corresponding to the full load condition.

(d) Material properties:
Young's modulus = 206 GPa,
Poisson's ratio = 0·3.

(e) Solution method:
linear and elastic analysis.

In order to compare the numerical results of deformations and stresses, the following quantities are evaluated;

(a) deformation pattern of the side structure,
(b) maximum deflection,
(c) deformation and stresses at SL 16,
(d) deformation and stresses at Fr. 72.

Since local stresses at the intersection of SL 16 and Fr. 72 are evaluated in the Phase-2 analysis, the bending and shearing components of stresses at SL 16 and Fr. 72, which are illustrated in Fig. 3, are calculated in the Phase-1 analysis.

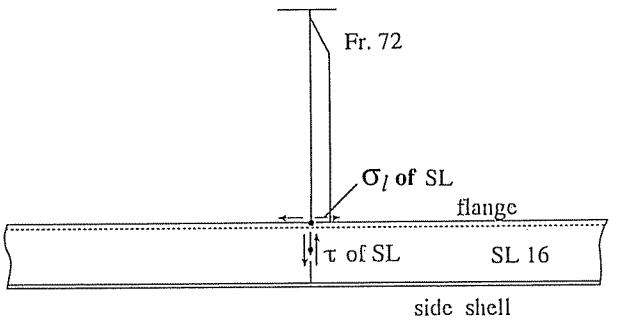

(a) Bending and shearing stresses of SLs.

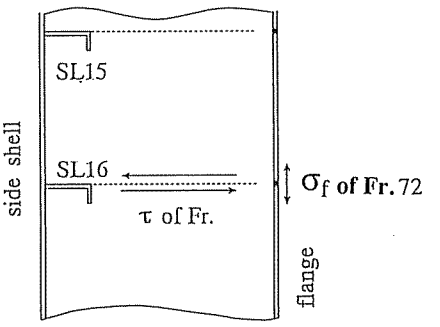

(b) Bending and shearing stresses of Frs.

Fig. 3. Location of calculated bending and shearing stresses.

2.2 Phase-2 analysis

The second phase of the study was the local stress analysis at the intersection of a transverse frame and a longitudinal stiffener. The solution sensitivities due to structural modeling, mesh refinement, and the application of boundary conditions to zoomed-up models are investigated in the comparative study. Based on the results of the Phase-1 analysis, a local structural model to investigate the stress concentration behavior at the intersection of SL 16 and Fr. 72 was defined by each contributor using his own solution procedure.

The local stresses are compared at the twelve points indicated in Fig. 4, where the points A–H are located on the top surface of the flange of SL 16, and the points I–L are located along the lower part of the transverse web stiffener of Fr. 72. Maximum (absolute value) principal stresses are evaluated in the present comparative study.

3 PHASE-1 COMPARATIVE STUDY

3.1 Structural idealization

The structural modeling, computer codes, and the total degrees of freedom are listed in Table 1, and the mesh patterns used are illustrated in Appendix A. The stiffened panel is modeled by a grillage structure in (1), while special stiffened panel elements are used in (10). Conventional finite element analyses were performed in the remaining analyses, where the shell plating is modeled by shell elements.

With regard to the modeling of transverse frames, whole frames are modeled by beam elements in (1), (3), (8) and (9), and by shell elements in (4) and (7), while the web and the flange are modeled by shell elements and by bar elements, respectively, in (2), (5), (6) and (11). In (2) and (6) the finite element models follow the frame shape near the deck and the bottom (see Figs A.2 and A.6). The web and the flange of the longitudinal stiffness are modeled by shell elements and bar elements, respectively, in (4) and (6), while the whole longitudinal stiffener is modeled by shell elements in (7). Beam elements are used for longitudinal stiffeners in the remaining analyses.

3.2 Results and discussions

A typical deformation pattern of the side structure is illustrated in Fig. 5, in which detailed deformation of some of the longitudinal stiffeners can be

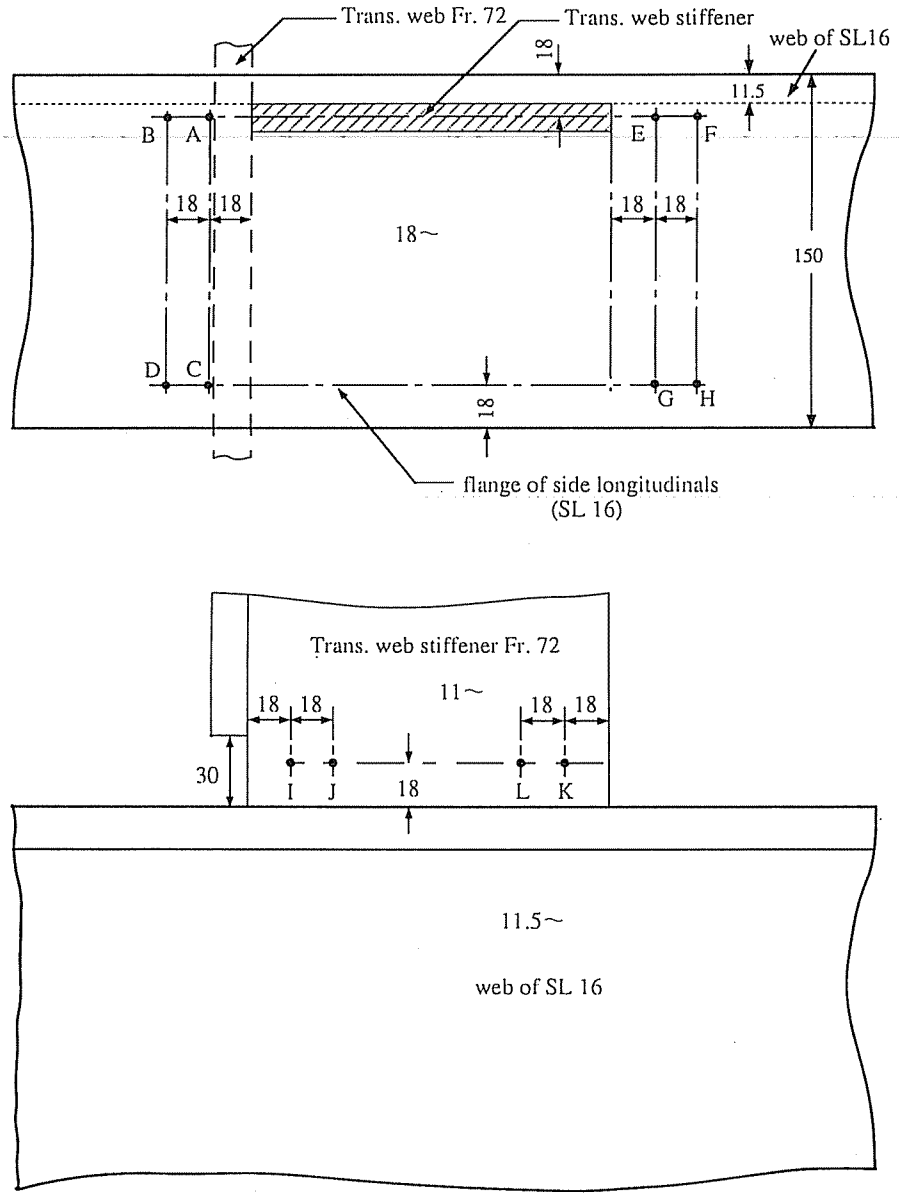

Fig. 4. Location of calculated local stresses.

evaluated (Ref. 4). A periodic nature of the deformation pattern is observed with respect to the transverse frames, and the maximum deflection at frames is attained at Fr. 69 and SL 16, and at Fr. 75 and SL 16. The results of the Phase-1 analyses are listed in Table 1, in which w is the

TABLE 1
Phase-1 Comparative Study

Contribution	*Modeling*			*Software*		*Total d.o.f.*	*Phase-1 results*		
	Side shell	*Longitudinals*	*Frames*	*Solver*	*Pre-post*		w (mm)	σ_f (MPa)	σ_1 (MPa)
(1)	beam	beam (grillage)	beam	ESTASY	MENTAT	932	1·29	15·1	−52·7
(2)	shell	beam	shell + bar	LUSAS	MYSTRO	1513 (nodes)	1·28	15·1	−53·3
(3)	shell	beam	beam	SHIPFEM	PATRAN	6948	1·47	31·1	−36·5
(4)	shell	shell/beam	shell	SESAM	PREFEM POSTFEM	30816	1·87	18·4	−78·5
(5)	shell	beam	shell + bar/ beam	VAST	VASTG	819 (half model)	1·61	25	−92
(6)	shell	shell + bar	shell + bar	SESAM	PREFEM POSTFEM	2898	1·21	18·1	−25·9
(7)	shell	shell	shell	COSMIC/ NASTRAN		(4000QUAD-4 elements)	—	—	—
(8)	shell	beam	beam	MSC/ NASTRAN (PC-version)		3397 (half model)	1·60	26·5	−49·5
(9)	shell	beam	beam	ANSYS	PATRAN	4800	1·58	23·8	−46·1
(10)	special stiffened elements			LBR-4		48 (6 elements)	1·69	27·1	−52·7
(11)	shell	beam	shell + beam	MSC/ NASTRAN	I-DEAS	4029	1·82	25·3	−39·6

deflection at the intersection of Fr. 72 and SL 16. The stresses, σ_f and σ_l are the bending stresses acting in the flanges of Fr. 72 and SL 16, respectively, at the intersection of these two members (see Fig. 3).

We can categorize the solutions into two groups corresponding to relatively smaller deflections [(1)–(3), (6)], and relatively larger ones [(4), (5), (7)–(11)]. It seems that the source of the difference stems mainly from the variety of supporting conditions at the struts; that is, supported by a single node, or by multiple nodes, and from the variety in structural idealization near the deck and the bottom. By using shell elements for the webs of transverse frames, the finite element models geometrically follow the frame shape near the deck and the bottom in (2) and (6). In cases (4) and (11), the rather large deformations include the effect of local deformation of the frame supported by a single node at the strut. The differences in the frame stress, σ_f, is closely related to the deformation characteristics.

Stresses, σ_l, at SL 16 show wide variations due to the structural models employed for the longitudinal stiffener. If more than four beam elements are used to model the longitudinal stiffener between the adjacent transverse frames, the bending stress without the warping effect can be represented automatically [(2) and (8)]. On the contrary, one beam element is enough, if the effect of the distributed load is explicitly taken into account (1). In the case where fine mesh subdivisions are carried out as shown in Fig. 5, the effects of warping of the longitudinal stiffeners and the local stress concentration at the member intersections may lead to very high stress levels [(4) and (5)], which approach those found in the Phase-2 detail analysis.

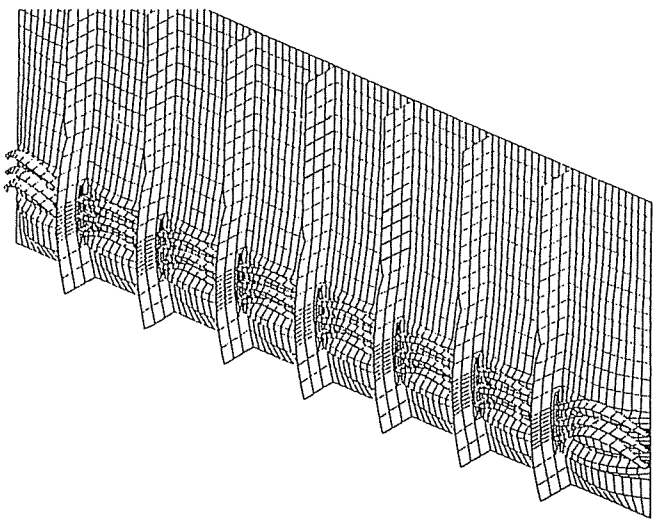

Fig. 5. Deformed side structure.

In most cases, the external water pressure is modeled as uniform pressure acting on each shell element. As far as the Phase-1 analyses were concerned, loading conditions were not a possible source of variation in the results.

Usually, global structural analyses are performed to examine the deformations and stresses of web frames, while the stresses in local strength members, such as those in longitudinal stiffeners, are evaluated by local strength analyses. Since procedures of detailed stress calculations are essential for the fatigue strength evaluation of structural details, the second phase of the comparative study examines stress concentrations at the three-dimensional intersection of structural members.

4 PHASE-2 COMPARATIVE STUDY

4.1 Structural modeling

The extent of the analyzed region, the application of the boundary conditions to the detailed model, computer codes, the total degrees of freedom and stress results are listed in Table 2, and the mesh patterns are illustrated in Appendix B.

Considering the approximately periodic nature of the deformation pattern with respect to frames in the middle part of the side structure, the global analysis models, which extend from SL 1 to SL 20 and from Fr. 71-1/2 to Fr. 72-1/2, are reconstructed in (3) and (4). In (4), a fine-meshed super-element is embedded in the vicinity of SL 16. Conventional zooming procedures are employed in the remaining analyses. As listed in Table 2, the extent of the analysis regions vary from two half bays to twice the transverse frame spacing in the ship length direction, while they vary from two half bays to (two + two halves) times the longitudinal stiffener spacing in the ship depth direction. The opening of the slot is disregarded in (2) and (4).

In relation to the finite element modeling, all contributors use shell elements, except for (5), where 3D solid elements are also used in the neighborhood of the member intersection. Relatively uniform mesh densities are observed except for (7) and (9) which use higher mesh densities.

The loading conditions applied to the structural analysis models are defined by the contributors' own procedures. A super-element technique is used in (4), while displacement boundary conditions and/or stress boundary conditions are specified based on Phase-1 analyses, in the rest of the analyses. Since not all of the boundary conditions of the zoomed-up models can be directly taken from the Phase-1 analyses, various methods were applied to derive the additional values.

TABLE 2
Phase-2 Comparative Study

Contribution	*Extent of analyzed region* { *frame direction*/ *longitudinal direction*	*Boundary conditions* { *fore and aft section of longitudinals*/ *upper and lower section of frames*	*Software*	*Total d.o.f.*	σ_A (MPa)	σ_E (MPa)
(1)	2 half bays/ 2 half bays	symmetric b.c./ stress b.c. from Phase 1	MARC	5717	−101	−82
(2)	2 half bays/ 2 half bays	displacement b.c. from Phase 1/ stress b.c. from Phase 1	LUSAS	1017 (nodes)	−127	−44
(3)	(2 + 2 halves) × longit. sp./ 2 half bays	stress b.c. from global model	SHIPFEM	13 565	−102	−70
(4)	(2 + 2 halves) × longit. sp./ 2 half bays	symmetric b.c./ supernodes to global model	SESAM	22 584	−94	−75
(5)	(2 + 2 halves) × longit. sp./ 2 half bays	displacement b.c. from Phase 1	VAST	20 255	−85	−60

(6)	2 bays/ 2 bays	displacement b.c. from Phase 1	SESAM	17952	−89	−57
(7)	2 bays/ 2 half bays	displacement b.c. from Phase 1	COSMIC/ NASTRAN	4000 (elements)	−101	−84
(8)	2 half bays/ 2 half bays	global displacement from Phase 1 symmetric b.c.	MSC/ NATRAN (PC version)	5742	−135	−75
(9)	2 half bays/ 2 half bays	stress b.c. from Phase 1	ANSYS	11016	−116	−88
(10)		Phase-1 analysis only				
(11)	2 bays/ 2 bays	displacement b.c. from Phase 1	MSC/ NASTRAN	9576	−107	−85

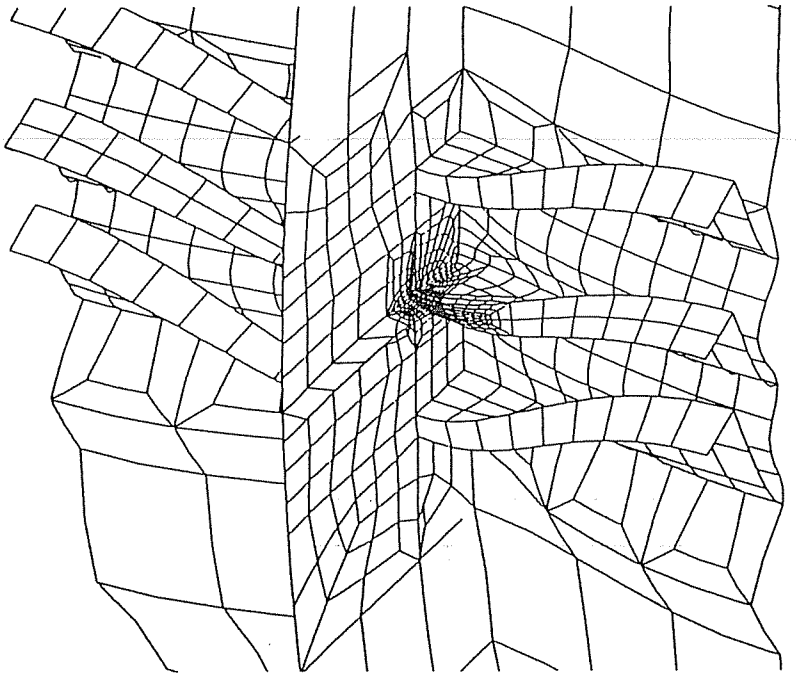

Fig. 6. Deformation in the vicinity of Fr. 72 and SLs 15–17.

4.2 Results and discussions

A typical deformation pattern at the intersection of a longitudinal stiffener and transverse frame is illustrated in Fig. 6 (Ref. 4), in which one can observe the significant effects of torsional bending of the asymmetric longitudinal stiffeners, and also the stress concentration at the connection of the stiffener flange and the transverse web stiffener.

High stress concentrations were calculated at points A and E on the flange of SL 16, and at points I and K on the transverse web stiffener. Maximum absolute values of stress are attained at point A with the absolute values having the relationships, $\sigma_A > \sigma_E$, $\sigma_I > \sigma_K$, in (1), (2), (4), (5), (8), (9) and (11). Higher stress is calculated in the transverse web stiffener, that is, $\sigma_I > \sigma_A$ in (3) and (6).

The Phase-2 results are listed in Table 2, in which stresses σ_A and σ_E are the absolute maximum principal stresses at points A and E, respectively (see Fig. 4). The results show a scatter of 25–30%. Differences in the extent of the analysis region and in the corresponding boundary conditions applied to the transverse frame and longitudinal stiffeners, modeling of the slot, and the mesh densities in the vicinity of the stress concentra-

tion regions, are possible sources of variation. Although the mesh density is relatively low in (11), similar stress levels were obtained in comparison with (7) and (9) by using proper mesh density in the vicinity of the stress concentration region.

In (3), analyses with both displacement boundary conditions and stress boundary conditions are examined. The displacement boundary condition gives lower stresses at all locations except at G and H, where the difference is less than 10% at all locations.

Since the effects of the relative deformation of the adjacent transverse frames can be disregarded in the middle part of the tank, the stress level at the intersection of the longitudinal stiffener and the transverse frame is mainly sensitive to the boundary conditions applied to the extreme parts of the transverse frame. The relative torsional deformation of the transverse frame, which may lead to additional localized stress concentrations at the intersection, could be a source of the wide variation in stress values. Where and how the stress values are calculated in the finite element code and in the post-processor are also likely causes of differences (i.e. stress smoothing algorithms, stress at nodes or integration points, etc.).

5 CONCLUSIONS

In the global structural analysis (Phase-1 analysis), the importance of the structural idealization in the vicinity of the supported boundary is recognized. It is obvious that the stresses in the longitudinal stiffeners are strongly affected by the element types and mesh subdivisions used.

In order to calculate the local stresses at the intersection of a transverse frame and a longitudinal stiffener, conventional zooming procedures are used in the majority of the present studies. It should be pointed out that not all of the deformation modes or tractions applied on the boundaries of the zoomed-up model could be defined in the previous global analyses, and that sometimes additional new members appeared in Phase-2 analysis. This means that a variety of hypotheses were introduced in the zoomed-up analyses which lead to different solutions. One way of resolving this problem would be to enlarge the zoomed-up region to extend to a couple of bays, both in ship length and in ship depth/breadth directions, so that the effects of the specific application of boundary conditions are reduced at the point of stress evaluation. One may also use the super-element (or substructuring) technique, where local models with fine-mesh subdivision are contained in a global model as

super-elements. This solution procedure may be efficient and effective when a structural designer knows in advance the exact parts of a structure where the local stress analyses should be carried out. One may further improve the accuracy of stress values in a stress concentration region by using an adaptive meshing technique, which is available in some commercial codes.

Some specific guidance on how and where stresses are to be calculated would improve consistency in results. This should be included in finite element guidelines. Results from this study are believed to be what is expected in current finite element analysis and point to a need for a more well defined unified approach for finite element analysis of ship structures. This is particularly important when the consequences are considered in fatigue analysis where small differences in stress values can lead to large changes in fatigue life estimates.

REFERENCES

1. Cervetto, D., Punta, F. & Zannetti, T., Finite element study of the side structure of a middle size tanker. Registro Italiano Navale, Genoa, Italy, 1993.
2. Das, P. K., Finite element study of the side structure of a middle size tanker. Department of Naval Architecture and Ocean Engineering, University of Glasgow, UK, 1993.
3. Hakala, M., Finite element study of the side structure of a middle size tanker. Technical Research Center of Finland, Espoo, Finland, 1993.
4. Loseth, R. & Verpe, T., Finite element study of the side structure of a middle size tanker. A. S. Veritas Research, Høvik, Norway, 1993.
5. Pegg, N., Finite element study of the side structure of a middle size tanker. Defence Research Establishment Atlantic, Dartmouth, Canada, 1993.
6. Fan, Y. & Senjanovic, I., Finite element strength analysis of tanker side structure. Faculty of Mechanical Engineering and Naval Architecture, University of Zagreb, Croatia, 1993.
7. Snyder, B. & Sielski, R., Finite element study of the side structure of a middle size tanker. Naval Surface Warfare Center, Carderock, Maryland, USA, 1993.
8. Sumi, Y., Finite element study of the side structure of a middle size tanker. Department of Naval Architecture and Ocean Engineering, Yokohama National University, Yokohama, Japan, 1993.
9. Wang, W., Finite element study of the side structure of a middle size tanker. Department of Naval Architecture, National Taiwan Ocean University, Keelung, Taiwan, China, 1993.
10. Rigo, P., Analytical study of the side structure of a middle size tanker. Naval Architecture and Transport System Department, University of Liege, Belgium, 1993.

11. Oppama Shipyard, Finite element study of the side structure of a middle size tanker. Sumitomo Heavy Industries, Yokosuka, Japan, 1993.
12. Ziliotto, F., Ebert, J., Hakala, M., Hong, D. P., Ivanov, L. D., Pegg, N. G., Sakato, T., Senjanovi, I. & Wang, W. H., Comparison of different finite element analyses of the transverse frame of a 350 000 TDW tanker. *Marine Structures* **4** (1991) 231–255.
13. Report of Committee II.1, Quasi-static load effects. *Proc. 11th ISSC,* Vol. 1. Elsevier Applied Science, 1991, pp. 214–218.
14. Report of Committee II.1, Quasi-static load effects. *Proc. 12th ISSC,* Vol. 1. 1994, pp. 151–231.

APPENDIX A

Finite element models for Phase-1 analyses

The finite element models used by the contributors are illustrated in Figs A.1–A.10.

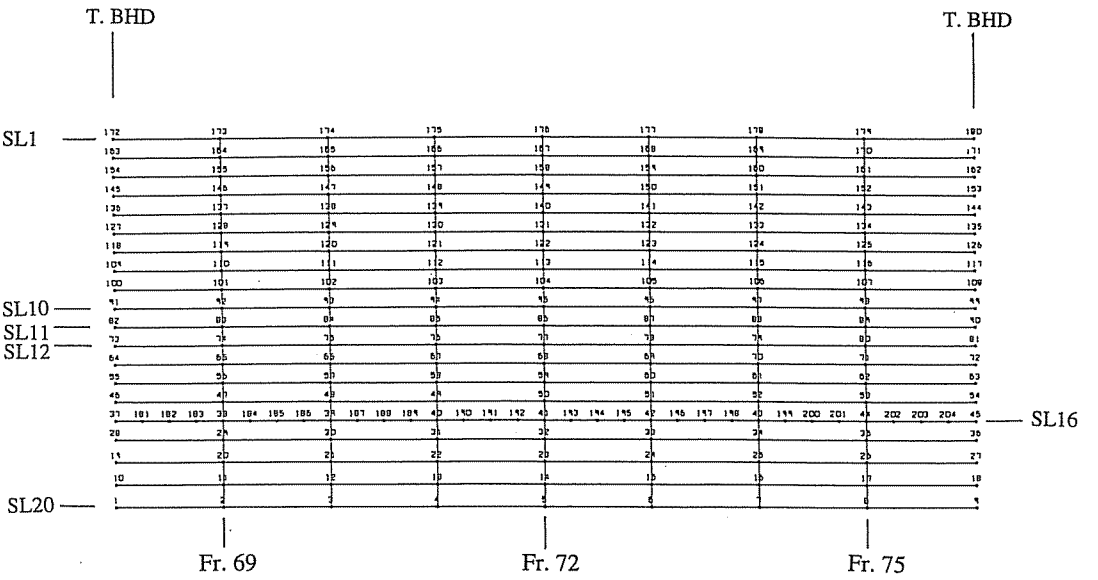

Fig. A.1. Grillage model of Analysis (1).

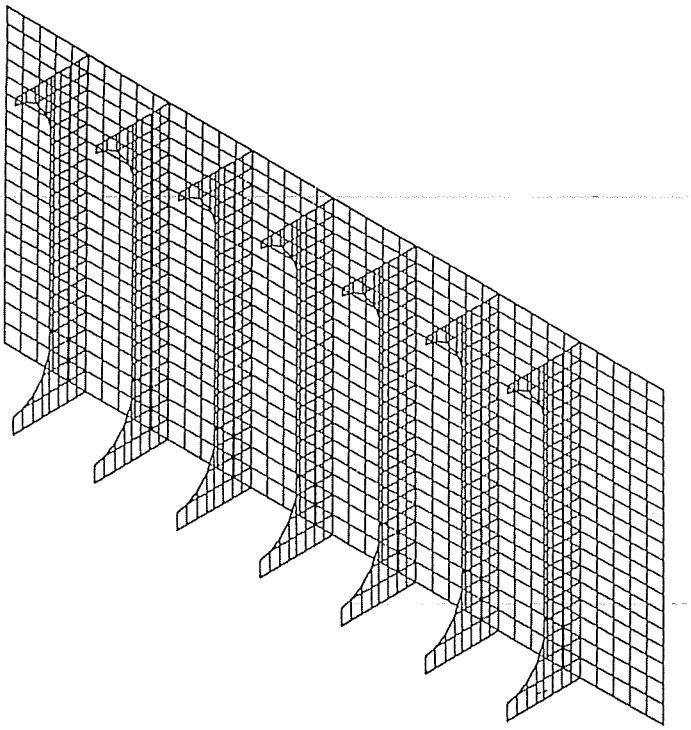

Fig. A.2. Finite element model of Analysis (2).

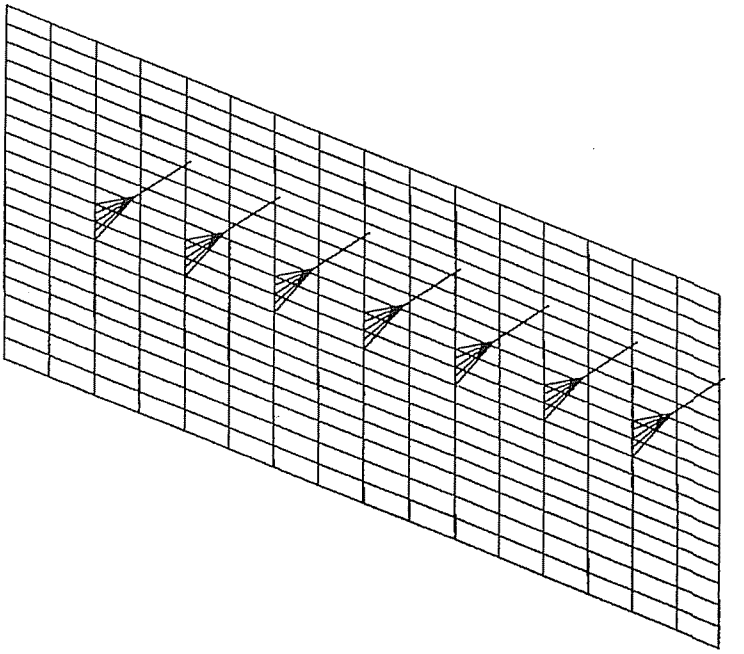

Fig. A.3. Finite element model of Analysis (3).

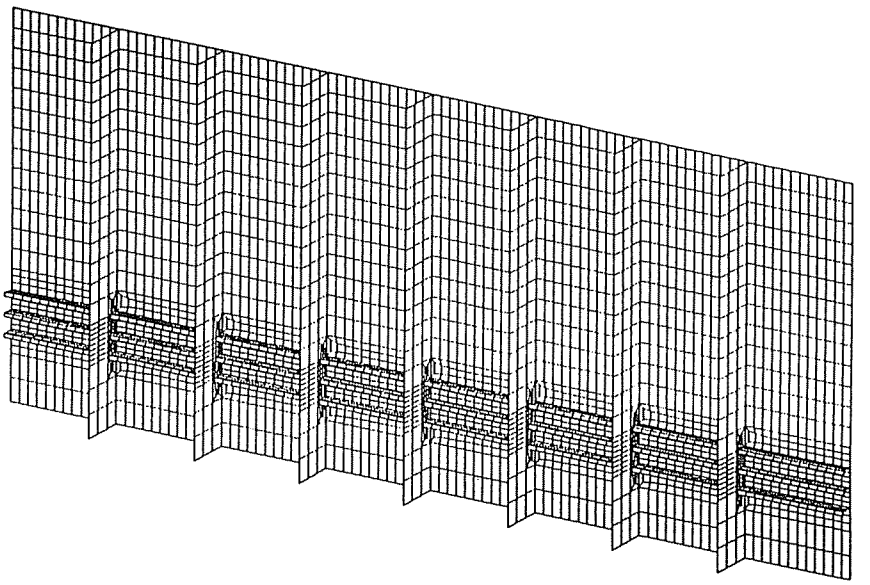

Fig. A.4. Finite element model of Analysis (4).

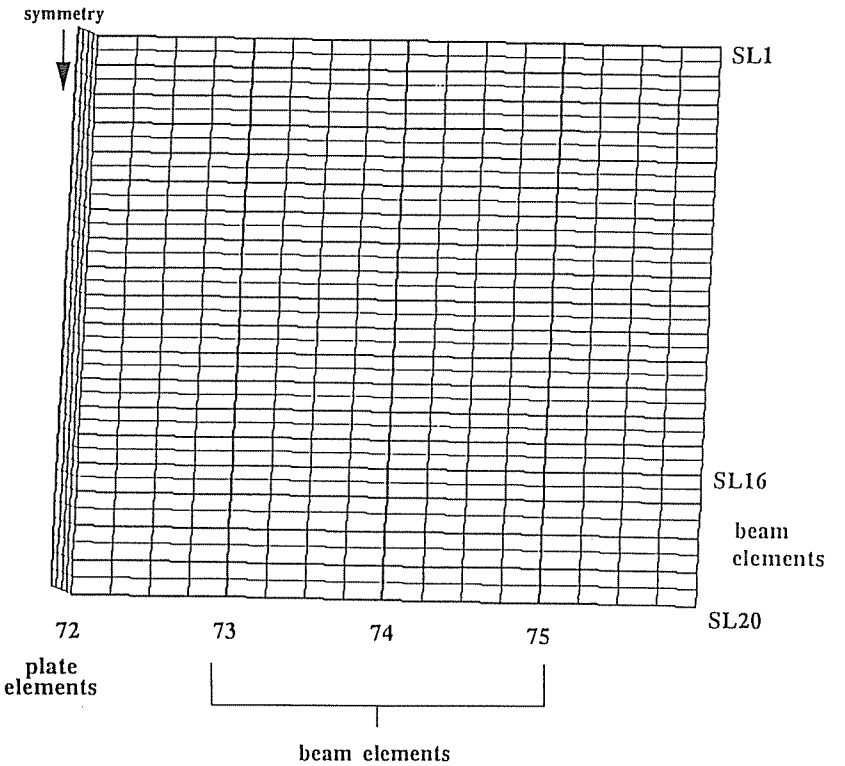

Fig. A.5. Finite element model of Analysis (5).

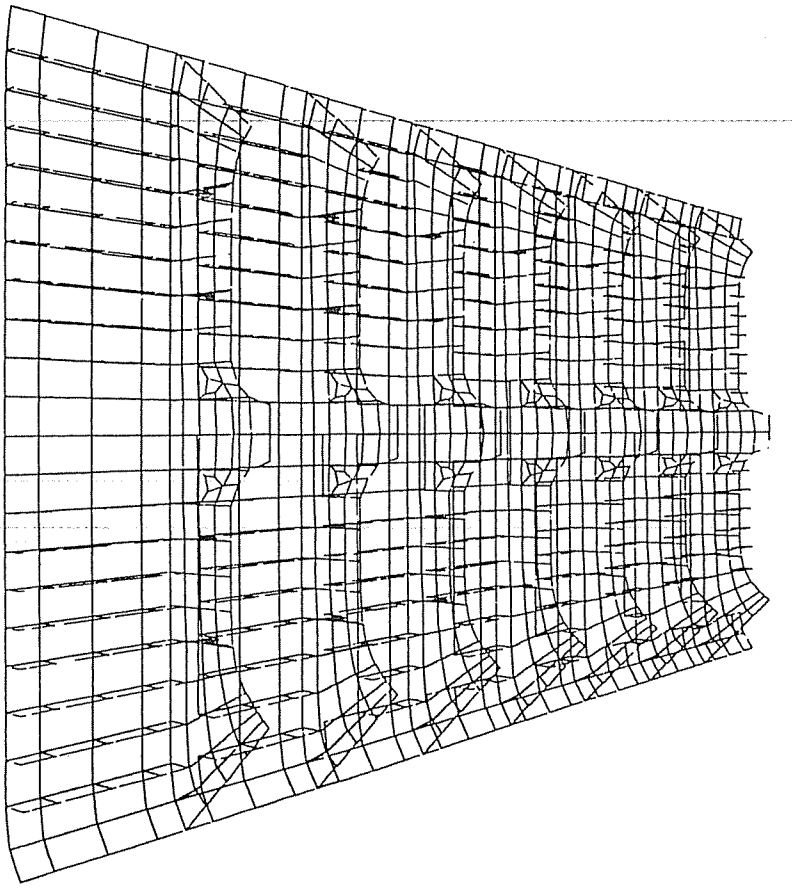

Fig. A.6. Finite element model of Analysis (6).

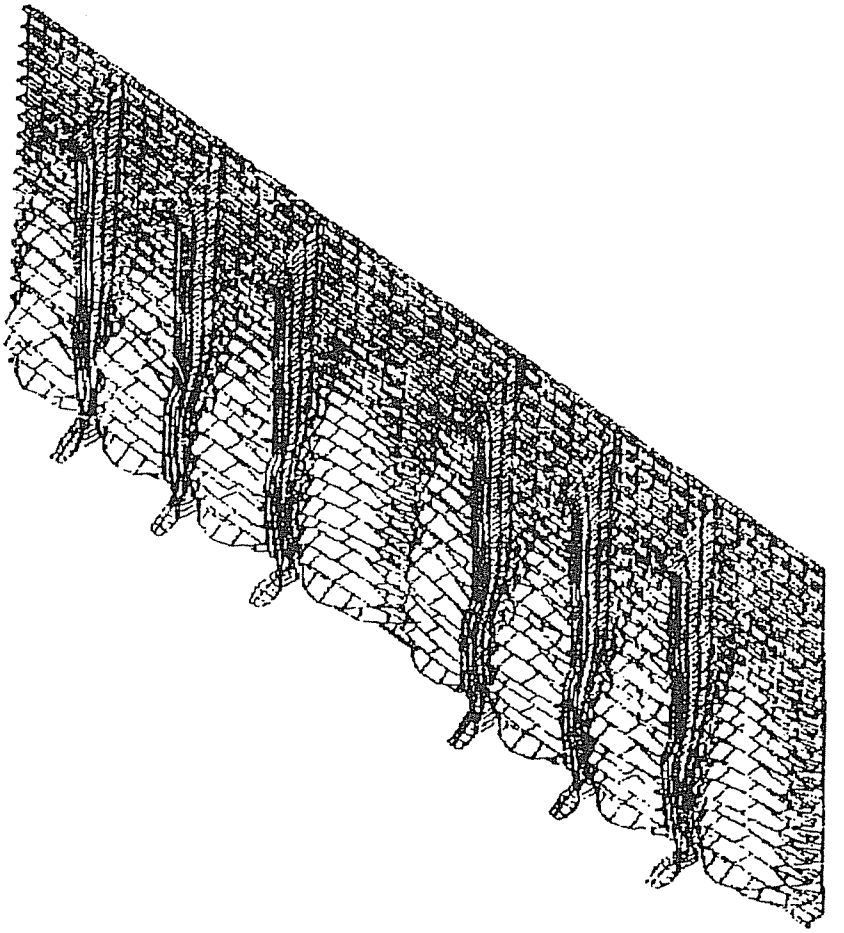

Fig. A.7. Finite element model and deformation of Analysis (7).

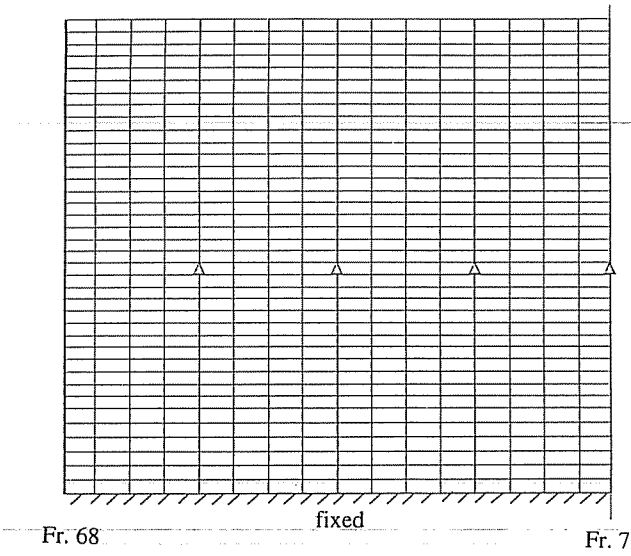

Fig. A.8. Finite element model of Analysis (8).

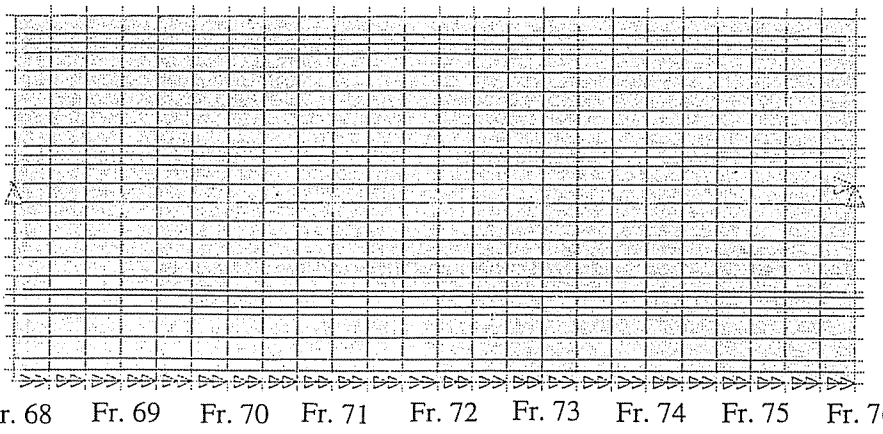

Fig. A.9. Finite element model of Analysis (9).

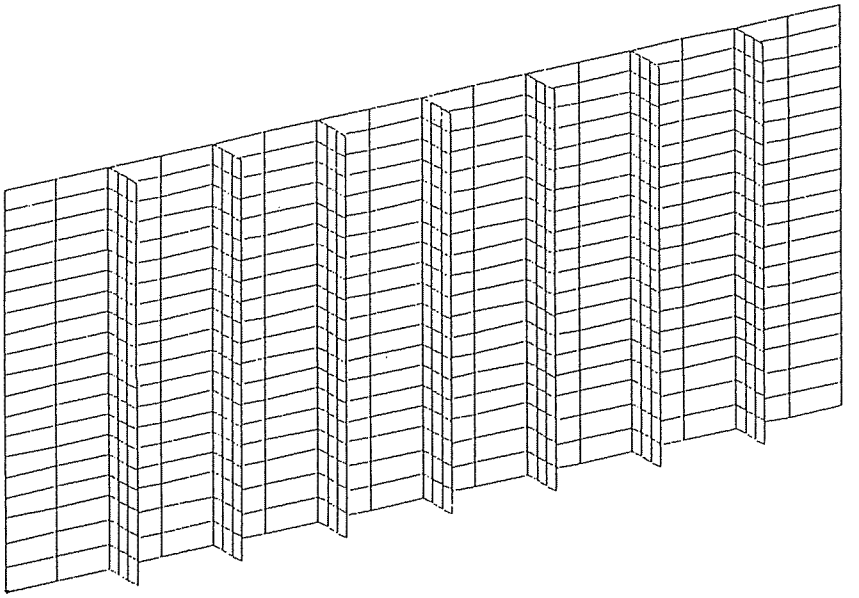

Fig. A.10. Finite element model of Analysis (11).

APPENDIX B

Finite element models for Phase-2 analyses

The finite element models used by the contributors are illustrated in Figs B.1–B.10, where the mesh pattern of the super-element of Fig. B.4 has been illustrated in Fig. 6.

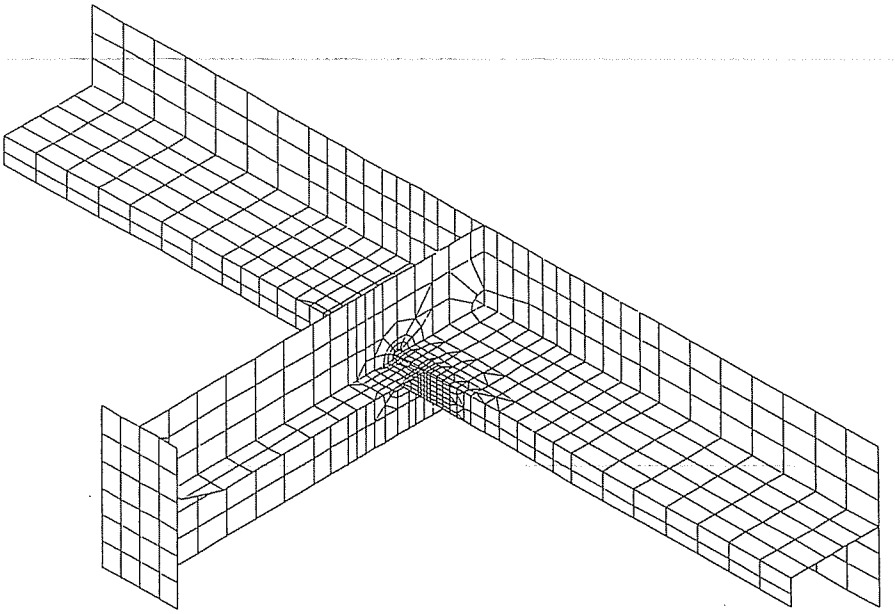

Fig. B.1. Finite element model of Analysis (1).

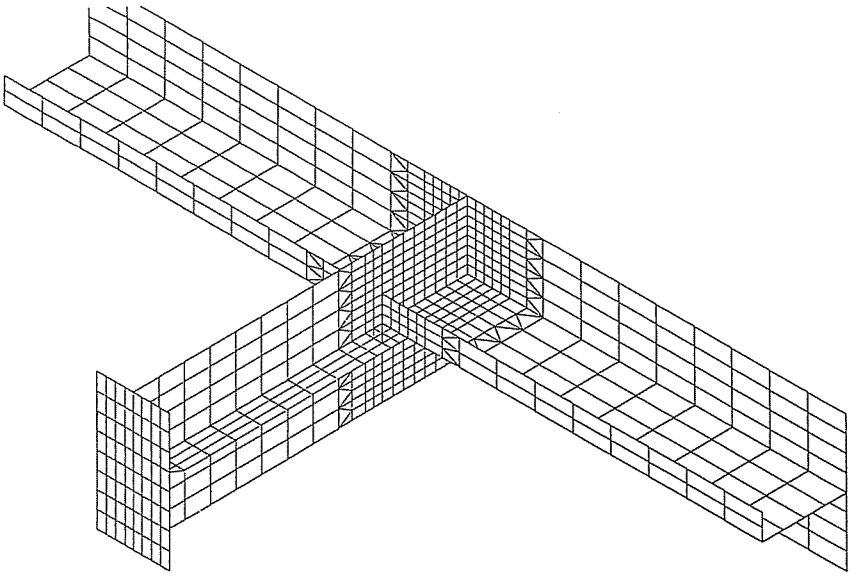

Fig. B.2. Finite element model of Analysis (2).

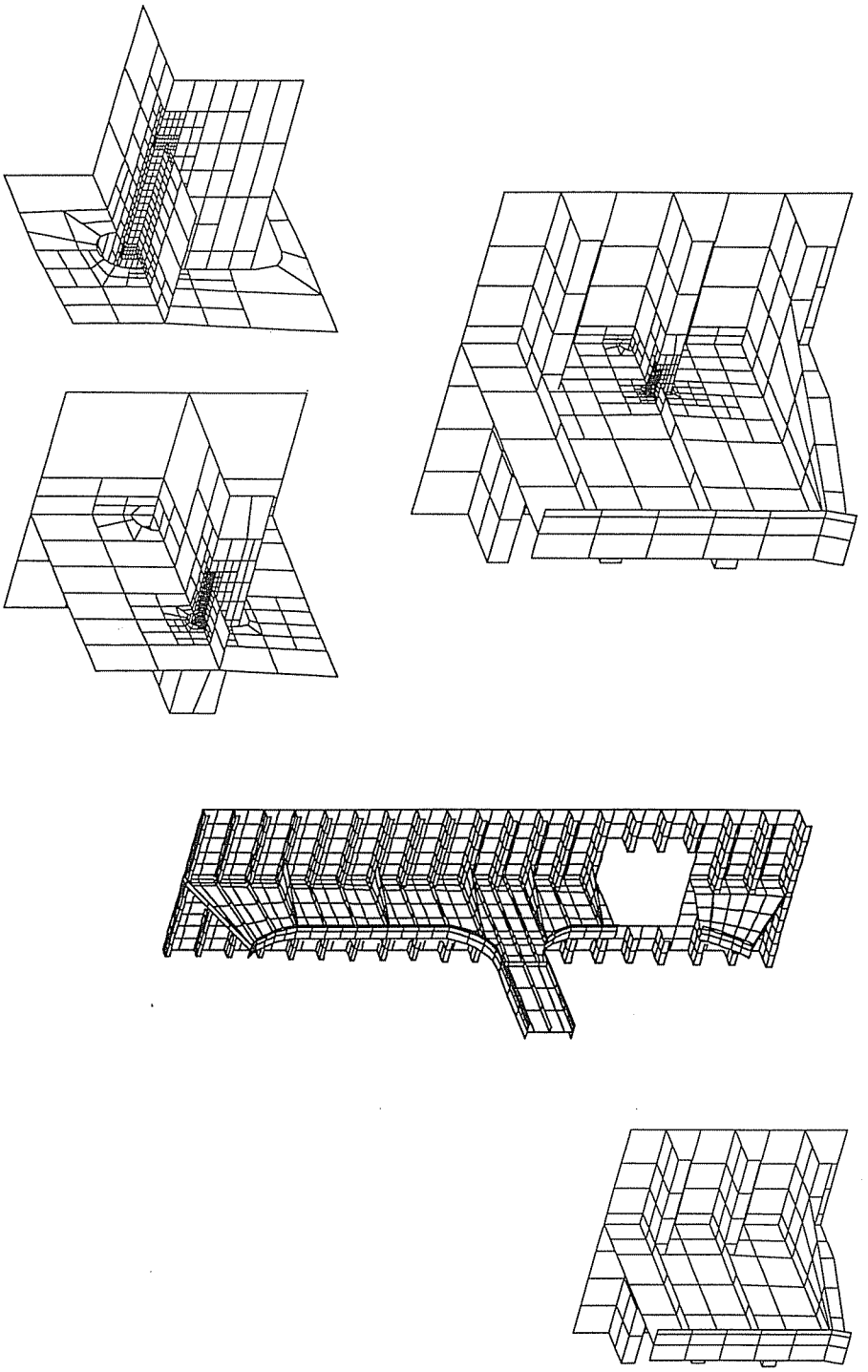

Fig. B.3(a). Global finite element model of Analysis (3), (b). Zoom-up model of Analysis (3).

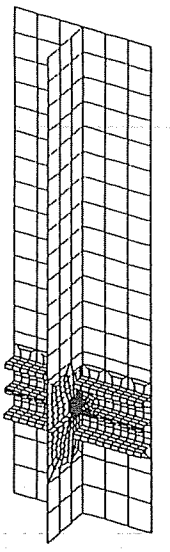

Fig. B.4. Finite element model of Analysis (4), in which a super-element is embedded near Fr. 72 and SL 16.

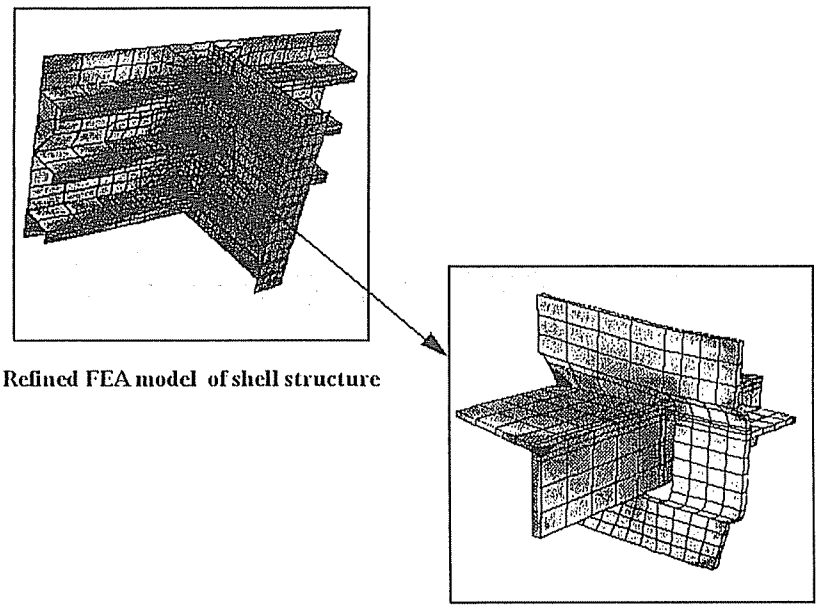

Fig. B.5. Finite element model of Analysis (5); modeling by shell elements and detail model by 3D solid elements.

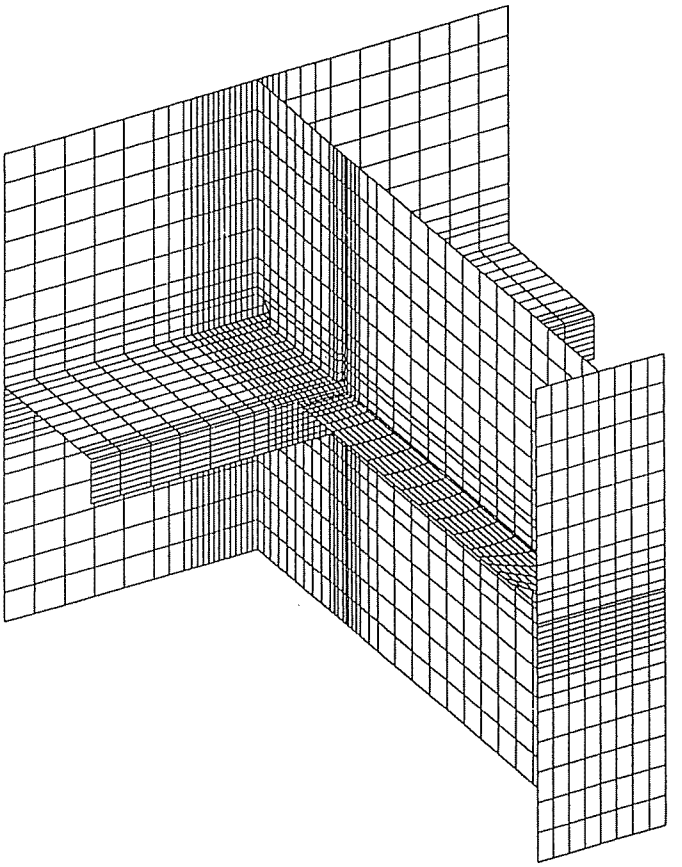

Fig. B6. Finite element model of Analysis (6).

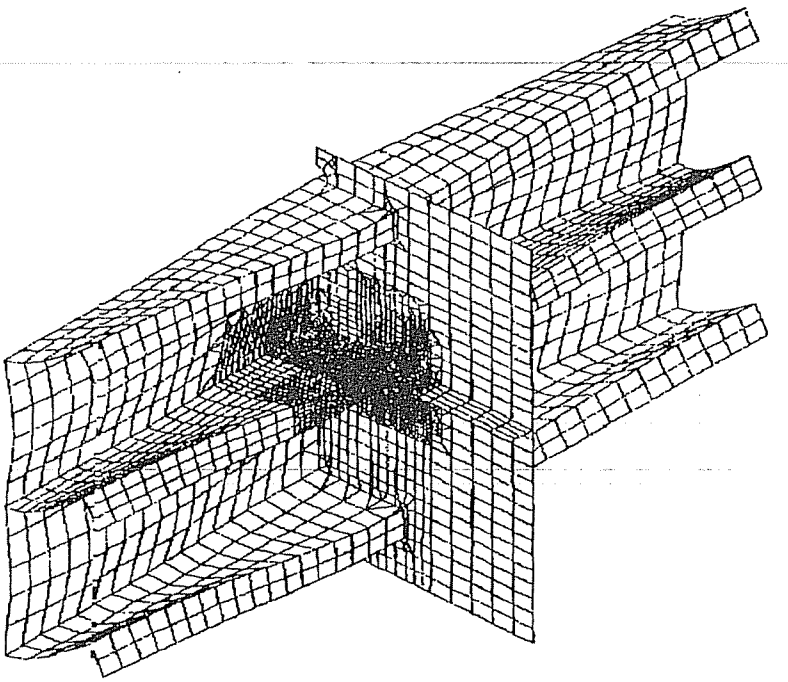

Fig. B.7. Finite element model and deformation of Analysis (7).

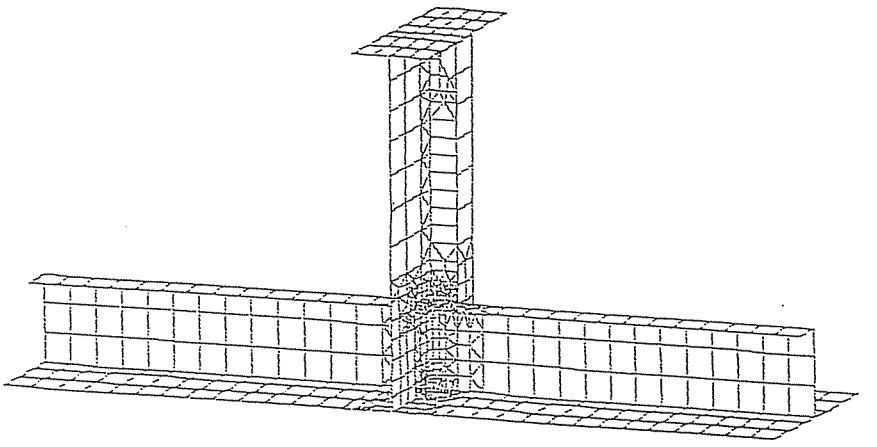

Fig. B.8. Finite element model of Analysis (8).

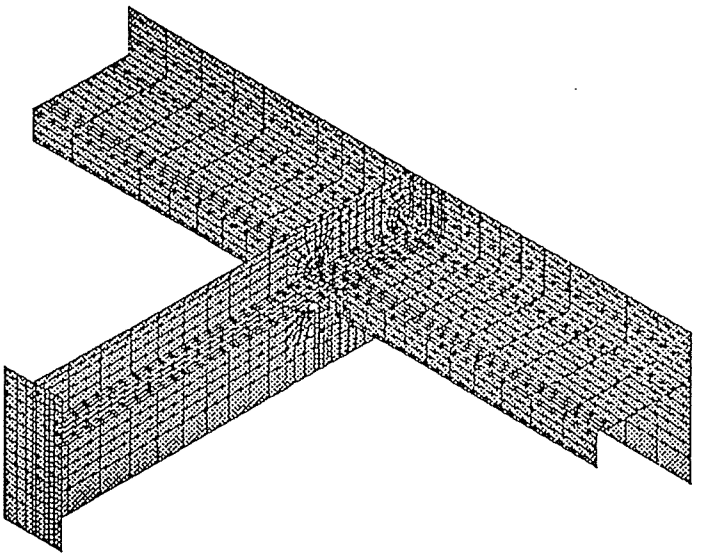

Fig. B.9. Finite element model of Analysis (9).

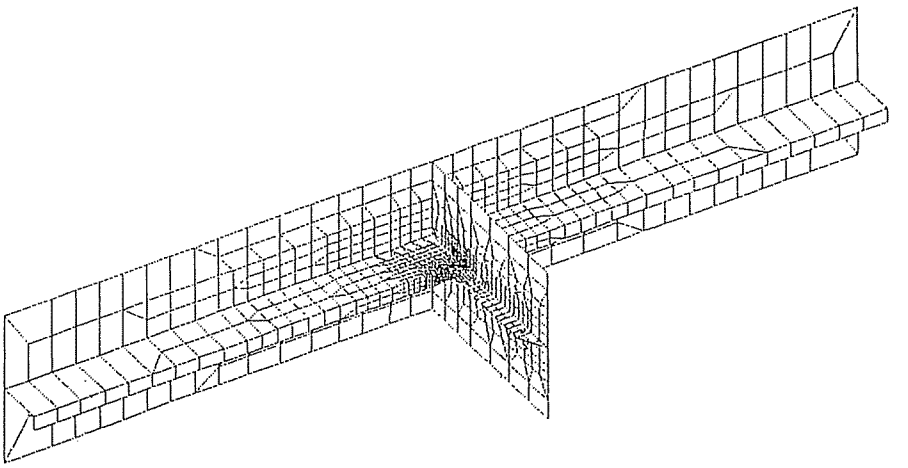

Fig. B.10. Finite element model of Analysis (11).